

See discussions, stats, and author profiles for this publication at: <https://www.researchgate.net/publication/264390186>

Majority logic gate for 3D magnetic computing

Article in *Nanotechnology* · July 2014

DOI: 10.1088/0957-4484/25/33/335202 · Source: PubMed

CITATIONS

38

READS

571

6 authors, including:



Irina Eichwald

Technische Universität München

35 PUBLICATIONS 431 CITATIONS

[SEE PROFILE](#)



Stephan Breitzkreutz-v. Gamm

Infineon Technologies

72 PUBLICATIONS 889 CITATIONS

[SEE PROFILE](#)



Grazvydas Ziemys

Technische Universität München

29 PUBLICATIONS 160 CITATIONS

[SEE PROFILE](#)



Wolfgang Porod

University of Notre Dame

377 PUBLICATIONS 9,137 CITATIONS

[SEE PROFILE](#)

Some of the authors of this publication are also working on these related projects:



Nanoelectronic circuits [View project](#)



Nanomagnetic Logic [View project](#)

Majority logic gate for 3D magnetic computing

This content has been downloaded from IOPscience. Please scroll down to see the full text.

2014 Nanotechnology 25 335202

(<http://iopscience.iop.org/0957-4484/25/33/335202>)

View [the table of contents for this issue](#), or go to the [journal homepage](#) for more

Download details:

IP Address: 129.187.254.46

This content was downloaded on 31/07/2014 at 07:33

Please note that [terms and conditions apply](#).

Majority logic gate for 3D magnetic computing

Irina Eichwald¹, Stephan Breitzkreutz¹, Grazvydas Ziemys¹, György Csaba², Wolfgang Porod³ and Markus Becherer¹

¹ Lehrstuhl für Technische Elektronik, Technische Universität München, Arcisstrasse 21, 80333 Munich, Germany

² Center for Nano Science and Technology, University of Notre Dame, 225A Cushing Hall, Notre Dame, IN 46556, USA

³ Center for Nano Science and Technology, University of Notre Dame, 203 Cushing Hall of Engineering, Notre Dame, IN 46556, USA

E-mail: irina.eichwald@tum.de


Received 2 May 2014, revised 3 June 2014

Accepted for publication 16 June 2014

Published 30 July 2014

Abstract

For decades now, microelectronic circuits have been exclusively built from transistors. An alternative way is to use nano-scaled magnets for the realization of digital circuits. This technology, known as nanomagnetic logic (NML), may offer significant improvements in terms of power consumption and integration densities. Further advantages of NML are: non-volatility, radiation hardness, and operation at room temperature. Recent research focuses on the three-dimensional (3D) integration of nanomagnets. Here we show, for the first time, a 3D programmable magnetic logic gate. Its computing operation is based on physically field-interacting nanometer-scaled magnets arranged in a 3D manner. The magnets possess a bistable magnetization state representing the Boolean logic states '0' and '1.' Magneto-optical and magnetic force microscopy measurements prove the correct operation of the gate over many computing cycles. Furthermore, micromagnetic simulations confirm the correct functionality of the gate even for a size in the nanometer-domain. The presented device demonstrates the potential of NML for three-dimensional digital computing, enabling the highest integration densities.

 Online supplementary data available from stacks.iop.org/NANO/25/335202/mmedia

Keywords: nanomagnetic logic, perpendicular magnetic anisotropy, 3D magnetic computing, 3D integration

(Some figures may appear in colour only in the online journal)

1. Introduction

Magnetic devices are widely known for data-storage applications. Here, information is stored in the magnetization state of ferromagnetic materials. Recent approaches focus on exploiting ferromagnetism in order to realize logic functionality [1–3]. Nanomagnetic logic (NML) is one of such possible approaches. Here, digital information is encoded in the bistable magnetization state of the nanomagnets. Magneto-static interactions between neighbouring magnets are exploited to propagate information and to realize magnetic computation, without the need of interconnects and electrical

wiring as in microelectronic circuits. NML is a low power technology [4] (typically $100 k_B T$ per switching process of a magnet, where k_B is the Boltzmann constant and T is the actual operating temperature), enabling the combination of memory and logic functionality in a single device [5].

A special areal arrangement of such field-interacting nanomagnets enables us to implement any arbitrary Boolean function. In the past, signal transmission through a chain of magnets [6–8], the functionality of a NAND/NOR gate [9, 10], and a full-adder circuit [11, 12] could be proven successfully. There are two kinds of NML: in-plane NML and perpendicular NML. In in-plane NML, the switching

behaviour of the magnets is dominated by the geometry of the magnet, the so-called ‘shape anisotropy’ being a constraint in the design parameter. In contrast, our group, and also others [13, 14], perform experiments on magnets with a perpendicular magnetic anisotropy (PMA). Here any shape can be chosen, saving this degree of freedom in the design of NML circuits [15]. The magnetic behaviour of such magnets is then tuned by focused ion beam (FIB) irradiation [16, 17]. Up to now, all logic functionality in NML was realized by a special arrangement of magnets lying in a single layer. This time, we use more than one functional layer and arrange magnets in a 3D manner to each other to achieve higher integration densities and more robustness. The 3D architecture allows us to place magnets in such a way to each other that the influence of the coupling fields can be exploited in a better way than for 2-dimensional (2D) architectures. In this paper, we present for the first time a 3D majority logic gate performing the logic operations NAND and NOR. The feasibility of 3D magnetic computing is demonstrated on the basis of the presented NAND/NOR gate, where magnets are placed above each other in more than one functional layer. The functionality of the gate is proven experimentally and supported by simulations. The presented gate opens the way for 3D architectures of NML circuits on a multi-level regime.

2. Methods

2.1. 3D NAND/NOR gate in perpendicular NML

In perpendicular NML, a magnetization vector pointing out of the film-plane represents the Boolean logic state ‘1.’ The opposed magnetization direction represents a logic ‘0.’ A NAND/NOR gate is composed of three input magnets I_1 , I_2 , I_3 surrounding an output magnet O (figure 1(a)). The magnetic stray fields k_1 , k_2 , k_3 emanating from the three inputs superpose. The output magnet aligns itself with the resulting net stray magnetic field. Input I_3 programs the functionality of the gate to either NOR or NAND. With I_3 tied permanently to a ‘1’ or ‘0’ state while I_1 and I_2 are switched between ‘1’ and ‘0,’ either a NOR or NAND operation is performed. In contrast to 2D, the 3D configuration has the third input I_3 located in a different functional layer.

2.2. Device fabrication

The fabrication process of the presented gate is illustrated in figure 1(b). We begin by sputtering a $(\text{Ti}_{1\text{ nm}}/\text{Pt}_{5\text{ nm}}/[\text{Co}_{0.6\text{ nm}}/\text{Pt}_{1\text{ nm}}]_{4x}/\text{Pt}_{3\text{ nm}})$ multilayer film on a silicon dioxide (SiO_2) substrate. In order to pattern the magnetic film, FIB lithography is used, followed by ion beam etching. Afterwards the magnets of the first layer are coated and planarized by a spin-on glass called hydrogen silsesquioxane (HSQ) [18]. As HSQ has similar properties to SiO_x [19], it is an adequate seed layer for the growth of further magnets in a second functional layer. Magnets of the second layer are fabricated from a $(\text{Ti}_{1\text{ nm}}/\text{Pt}_{5\text{ nm}}/[\text{Co}_{0.6\text{ nm}}/\text{Pt}_{1\text{ nm}}]_{5x}/\text{Pt}_{3\text{ nm}})$ multilayer film, which is sputtered on the HSQ-layer. The second

film is again structured by FIB lithography, followed by ion beam etching. The vertical distance between magnets of the two functional layers accounts to 60 nm.

As magnetic field coupling is non-reciprocal, we have to make sure that only the three inputs influence the output magnet and not vice versa. Otherwise, correct functionality of the device cannot be guaranteed. Therefore we use local FIB irradiation. A small area ($40\text{ nm} \cdot 40\text{ nm}$) of the output O is irradiated by $1 \cdot 10^{14} \frac{\text{Ions}}{\text{cm}^2}$ using a 50 kV Ga^+ FIB. The irradiation destroys the crystalline structure, leading to a highly reduced anisotropy [20–22] in the irradiated spot. This spot is an easy nucleation region for a domain wall, which reverses the whole magnet by propagating through the magnet. If this irradiated spot is placed sufficiently close ($\leq 100\text{ nm}$) to surrounding magnets, domain wall nucleation can be prohibited or evoked by the stray fields from surrounding magnets. This way, magnetization reversal of the irradiated output magnet is controlled by the stray fields from the surrounding three inputs I_1 , I_2 , I_3 acting in the irradiated spot [17]. Our gate is constructed so that the strength of the stray fields of the three inputs is the same. This ensures equal influence of the inputs on the output magnet. A SEM image of the gate is shown in figure 1(c). The size of the magnets is in the $\mu\text{ m}$ regime to enable magneto-optical Kerr Effect (MOKE) measurements (resolution of our MOKE microscopy is limited to $\approx 1\text{ }\mu\text{ m}$). We use MOKE to verify correct functionality of the gate. Nevertheless, the whole computing area of the gate accounts to only $\approx 700\text{ nm} \cdot 550\text{ nm}$ (see figure 1(c) magnified extract).

2.3. Switching behaviour of field-coupled magnets

The three input magnets influence the switching behaviour of the output magnet by their emanating stray fields. This influence becomes apparent in the switching field values of the output magnet. The following consideration explains this fact:

A single magnet O is switched in the ‘1’ and ‘0’ state, applying an external field H_{Ext} perpendicular to the film-plane (see figure 2(a)). Without the influence of stray fields from surrounding magnets, the switching of O is symmetrical at the $\pm H_{\text{Switch}}$. In the presence of stray fields from surrounding magnets, the switching field amplitude of O is shifted to higher or lower values (see figure 2(b)). Whenever O is switched in parallel to the net stray field k_{Net} (sum of stray fields emanating from the inputs I_1 , I_2 , I_3), the external field coincides with k_{Net} , and the switching field amplitude is reduced by the amount of k_{Net} . The switching of O in the anti-parallel state to k_{Net} is inhibited, as k_{Net} counteracts to the applied external field. In this case, the influence of k_{Net} is overcome by a switching field amplitude increased by the amount of k_{Net} .

3. Results

3.1. Magneto-optical Kerr-effect measurements

We measured the influence of k_{Net} on the switching behaviour of O to verify the correct functionality of the gate. Therefore,

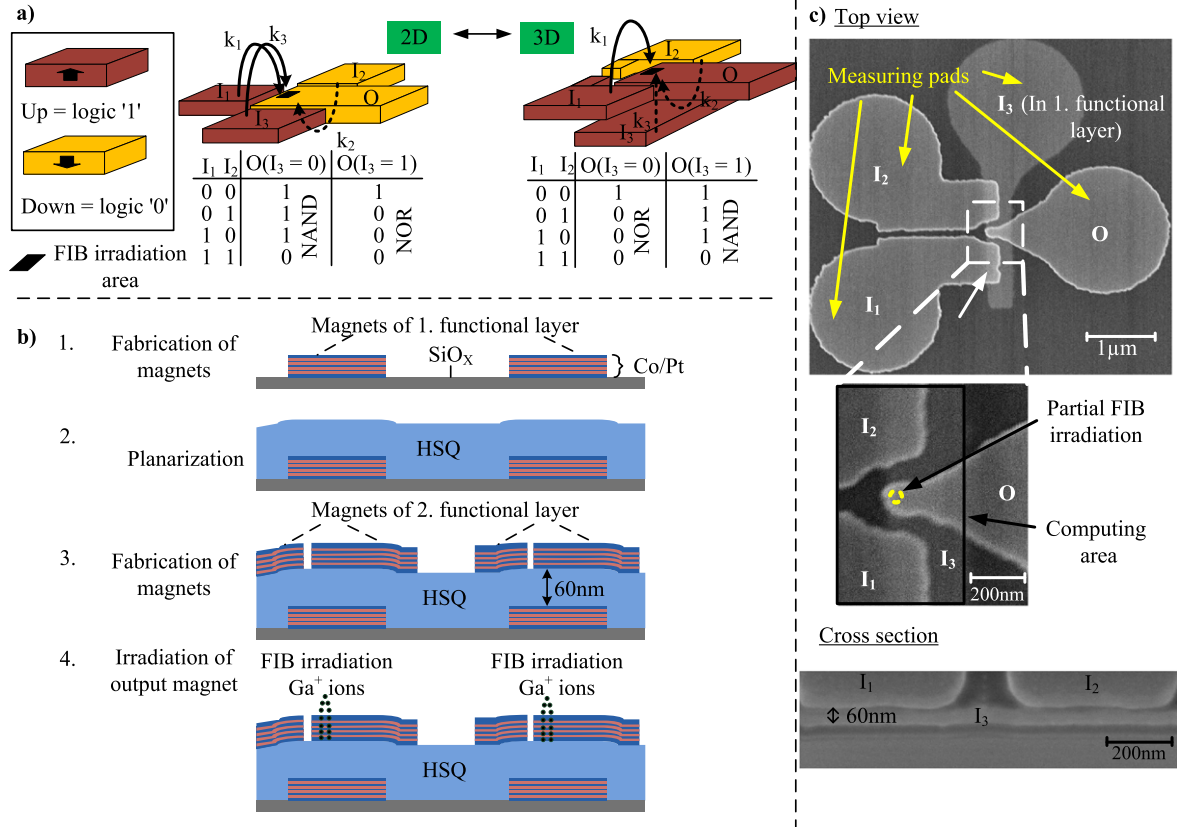


Figure 1. Schematics, fabrication steps, and SEM image of NAND/NOR gate. (a) Comparative schematic of a 2D and 3D NAND/NOR gate. Output O aligns with the net stray field, being the sum of the stray fields k_1 , k_2 , and k_3 emanating from the inputs I_1 , I_2 , I_3 . (b) Fabrication steps for 3D NAND/NOR gate. Magnets of the first and second functional layer are separated by 60 nm of HSQ. (c) SEM image of the fabricated gate. Input I_3 is located in the first functional layer, while the rest of the magnets lie in the second functional layer.

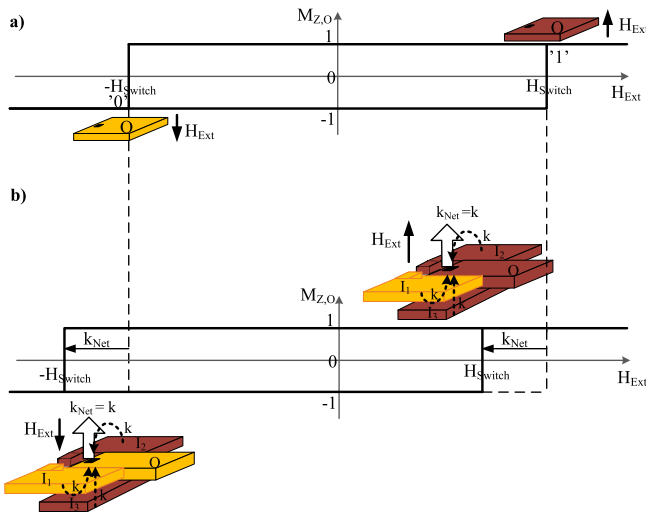


Figure 2. Schematic of the switching behaviour of a field-coupled nanomagnet. (a) Symmetrical switching of a single magnet O. (b) Asymmetrical switching of a field-coupled magnet O, influenced by the net stray field k_{Net} emanating from the inputs I_1 , I_2 , I_3 .

we set the inputs I_1 , I_2 , I_3 to one of the possible eight input configurations and switched O in turns in the parallel and anti-parallel state to the resulting k_{Net} . The non-irradiated inputs provide different switching field amplitudes (μ_0

$H_{Switch,I_1} = 153$ mT, $\mu_0 H_{Switch,I_2} = 122$ mT, $\mu_0 H_{Switch,I_3} = 105$ mT), due to variations in the fabrication process [23] of the film they are composed of. Therefore, the inputs of the gate can be set independently by different external field amplitudes, beginning with the highest one and finishing with the lowest one. As the output magnet is irradiated, it has a much smaller switching field amplitude than the inputs [6]. Therefore it is possible to switch and investigate the output without changing the input magnetization configuration.

The MOKE was used to record the magnetization state of O in dependency of the applied external field (Hysteresis loop). The results are shown in figure 3(a).

As expected, the input configurations $\{I_1 I_2 I_3\} \in \{000, 001, 011, 101\}$ shift the switching field values of O to the left. These input configurations produce a k_{Net} pointing out of the plane. Here, the switching of O in the '1' state (parallel to k_{Net} , the correct state) is facilitated by k_{Net} , resulting in reduced switching field amplitudes $\in [36$ mT; 45 mT]. Switching in the '0' state (anti-parallel to k_{Net} , the incorrect state) is inhibited by k_{Net} , resulting in enhanced switching field amplitudes $\in [-68$ mT; -56 mT].

For input configurations $\{I_1 I_2 I_3\} \in \{010, 100, 110, 111\}$, the switching field values are shifted to the right. As these input configurations produce a k_{Net} pointing into the plane, the switching of O in the '0' state (parallel to k_{Net} , the correct state) is facilitated, resulting in reduced switching field

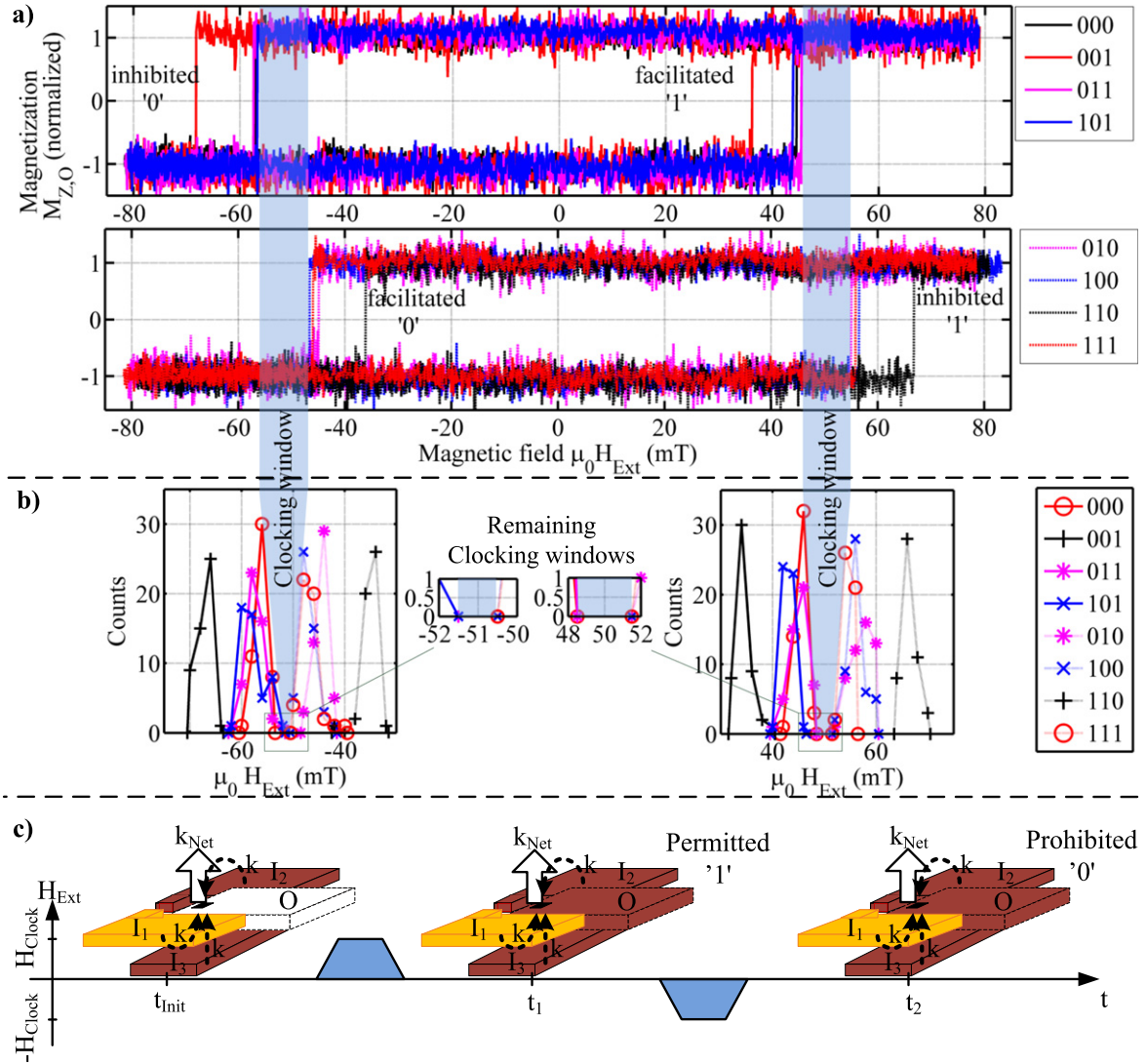


Figure 3. Measurement results with schematic of gate clocking. (a) Hysteresis loops of O for the eight possible input configurations of I_1 , I_2 , I_3 . (b) Switching field distributions of O for 50 switching cycles per input configuration of I_1 , I_2 , I_3 . (c) Applying a clocking field, k_{Net} aligns O in the correct state, while the incorrect state is prohibited by k_{Net} .

amplitudes $\in [-46 \text{ mT}; -36 \text{ mT}]$. Switching in the '1' state (anti-parallel to k_{Net} , the incorrect state) is inhibited, resulting in enhanced switching field amplitudes $\in [55 \text{ mT}; 66 \text{ mT}]$. Furthermore, it is obvious that the shift is the highest for the input configurations $\{I_1 I_2 I_3\} \in \{001, 110\}$, as the sum of the input stray fields is maximal and therefore k_{Net} .

Applying an alternating external field with amplitudes in between facilitated and inhibited switching of O (see figure 3 clocking window), the magnetization state of O is always calculated correctly by the influence of k_{Net} after one clocking cycle, at the latest. In figure 3(c), one clocking cycle for the input configuration $\{I_1 I_2 I_3\} \in \{011\}$ is exemplarily shown. In the initial state, the magnetization state of O is unknown. Applying a positive H_{Clock} , O aligns with the resulting k_{Net} in the permitted '1' state. Applying a negative H_{Clock} , H_{Clock} is not sufficient to overcome the influence of k_{Net} , and therefore switching in the '0' state cannot happen.

Due to the presence of thermal noise, the switching field of a magnet is distributed over time [23, 24]. It is expected

that for a high number of switching cycles per input configuration, the switching field values of O vary in a certain range. These variations narrow the clocking window. To guarantee the correct functionality of the gate, even in the presence of thermal noise, we repeated our experiments for 50 switching cycles of O for each input configuration. The resulting switching field distributions are shown in figure 3(b), and the mean switching field values are summarized in table 1. Regarding the obtained mean switching field values from table 1, they indicate a clocking window of 8 mT (the difference between the required maximum amplitude when a '1' or '0' is desired and the minimum amplitude when a '1' or '0' would occur erroneously). Indeed, figure 3(b) reveals that due to thermal noise, the clocking window is narrowed significantly (in the range of 50 mT–52 mT). Nevertheless, the switching field distributions obtained for the input configurations $\{000, 001, 011, 101\}$ and $\{010, 100, 110, 111\}$ are still separated from each other, proving the correct functionality of the gate. In the case of

Table 1. Mean switching field values of O for all input configurations.

Input			Output O		Clocked O
I ₁	I ₂	I ₃	$\mu_0 H_{\text{Switch}}(O \mapsto 0)$	$\mu_0 H_{\text{Switch}}(O \mapsto 1)$	
0	0	0	-57 mT	45 mT	1
0	0	1	-67 mT	36 mT	1
0	1	1	-57 mT	44 mT	1
1	0	1	-57 mT	43 mT	1
0	1	0	-45 mT	56 mT	0
1	0	0	-46 mT	56 mT	0
1	1	0	-37 mT	67 mT	0
1	1	1	-45 mT	54 mT	0

overlap, there is no clocking window left (meaning that it cannot be clearly distinguished between the correct and incorrect magnetization state of the output), and the gate cannot be clocked correctly.

The strength of k_{Net} is calculated by the sum of the stray fields emanating from the input magnets. For the presented gate, the stray field of each input I_x (with $x \in (1, 2, 3)$) can be determined from the difference of the mean switching field values (summarized in table 1) of O, where $I_x = 1$ and $I_x = 0$:

$$2 \cdot k_{I_x} = \left(\sum_{i=1}^8 H_{\text{Switch}}(I_x = 1) - \sum_{i=1}^8 H_{\text{Switch}}(I_x = 0) \right) / 8. \quad (1)$$

Resolving 1, we get: $k_{I_1} = |5 \text{ mT}|$, $k_{I_2} = |5.25 \text{ mT}|$, $k_{I_3} = |5 \text{ mT}|$.

The values reveal that the influence of each input varies by 5%. Depending on the input configurations, the maximum k_{Net} can reach up to 15.25 mT, and the minimum k_{Net} is 4.75 mT.

3.2. Magnetic force microscopy measurements

We acquired high-resolution images of the magnetization states of all four magnets by magnetic force microscopy (MFM). The images reveal that for every input configuration, after one clocking cycle with the clocking amplitude of 51 mT, the magnetization state of O was set correctly by the resulting k_{Net} (see figure 4).

3.3. Micromagnetic simulations

Furthermore, we performed micromagnetic simulations [25] to determine the computing area of the gate (see figure 1(c) computing area). The computing area of the gate considers only the magnetic area of the inputs (smaller than their original size) required to produce the measured stray field values. The simulations show that the required computing area amounts to $\approx 700 \text{ nm} \cdot 550 \text{ nm}$, leading to the measured stray field values and therefore correct functionality of the gate (see figure 5). The magnetic material of the inputs outside the computing area

contributes less than 1% to the resulting stray field. It is therefore negligible for the correct functionality of the gate and is only required for our MOKE measurements (for details see supplementary information). Thus, the presented gate can be scaled down to this nm-domain.

4. Discussion

4.1. Error rates and critical parameters

The error rate of the presented gate was calculated to be 4% (worst-case approximation). An error only occurs when the switching field distributions of the output magnet O, resulting from the input configurations $\{I_1 I_2 I_3\} \in \{000, 001, 011, 101\}$, overlap with the switching field distributions resulting from the input configurations $\{I_1 I_2 I_3\} \in \{010, 100, 110, 111\}$. Therefore each switching field distribution was fitted by a Gaussian curve using the MATLAB Curve Fitting tool (least square fit), and the probability for an overlap was determined from the resulting curves and the related standard deviations (for details see supplementary information).

Our experiments revealed that the strength of k_{Net} is crucial for the correct functionality of the gate. It defines the width of the clocking window. The strength of k_{Net} can be enhanced by several parameters, leading to a wider clocking window and therefore to a smaller error rate and higher robustness of the gate:

(a) Increase the amount of ferromagnetic material that the nanomagnets are composed of; e.g., increase the number of multilayers or use Co/Ni as a multilayer [7]. k_{Net} increases proportionally with an increasing amount of ferromagnetic material.

(b) Decrease the distance between the input magnets and the irradiated spot of the output magnet. k_{Net} is \approx inversely proportional to the distance.

(c) Increase the amount of magnetic material surrounding the output magnet. This possibility is already provided by our presented 3D architecture of the NAND/NOR gate, leading to a high robustness of the 3D gate. The location of the third input in an extra functional layer in comparison to 2D NAND/NOR enables us to enhance the amount of magnetic area surrounding the output magnet by 1/3. The influence of each input magnet is then increased by 1/6, and the same is k_{Net} .

For the presented gate, we calculated that k_{Net} has to be increased up to 8.5 mT to result in an error rate $\leq 0.01\%$. This can be achieved by following the suggestions given in (a), (b), and (c).

4.2. Vision of a 3D magnetic signal processing system

We demonstrated, on the basis of the NAND/NOR gate, that magnetic logic computing is possible on a multilevel regime. In figure 6, we propose a 3D architecture for a whole magnetic computing circuitry. To set the magnetization state of an input magnet (here A), a current driven wire is used [26]. To transmit information from one point to another in the nanomagnetic circuit (e.g., from A to I₁), magnets are ordered in chains [7, 8]. Logic operation is performed, for example, by

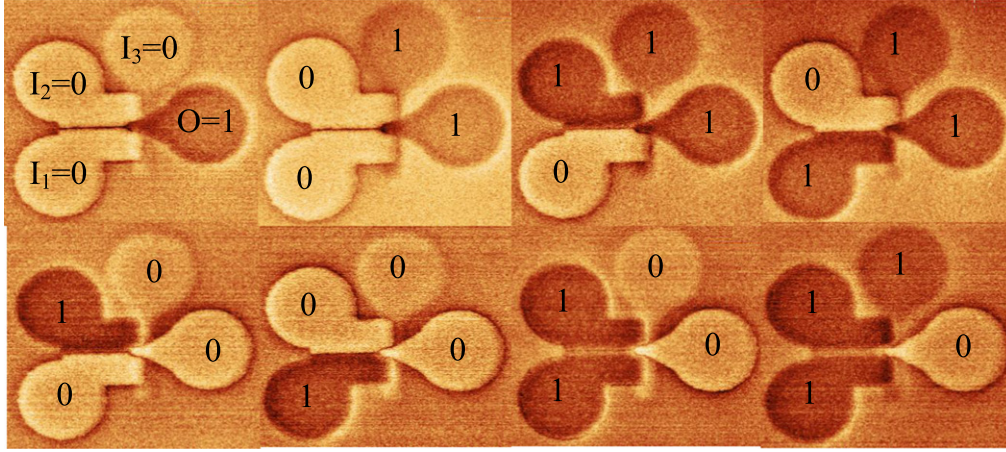


Figure 4. MFM images. Magnetization states of O for all input configurations (temporally after one clocking cycle).

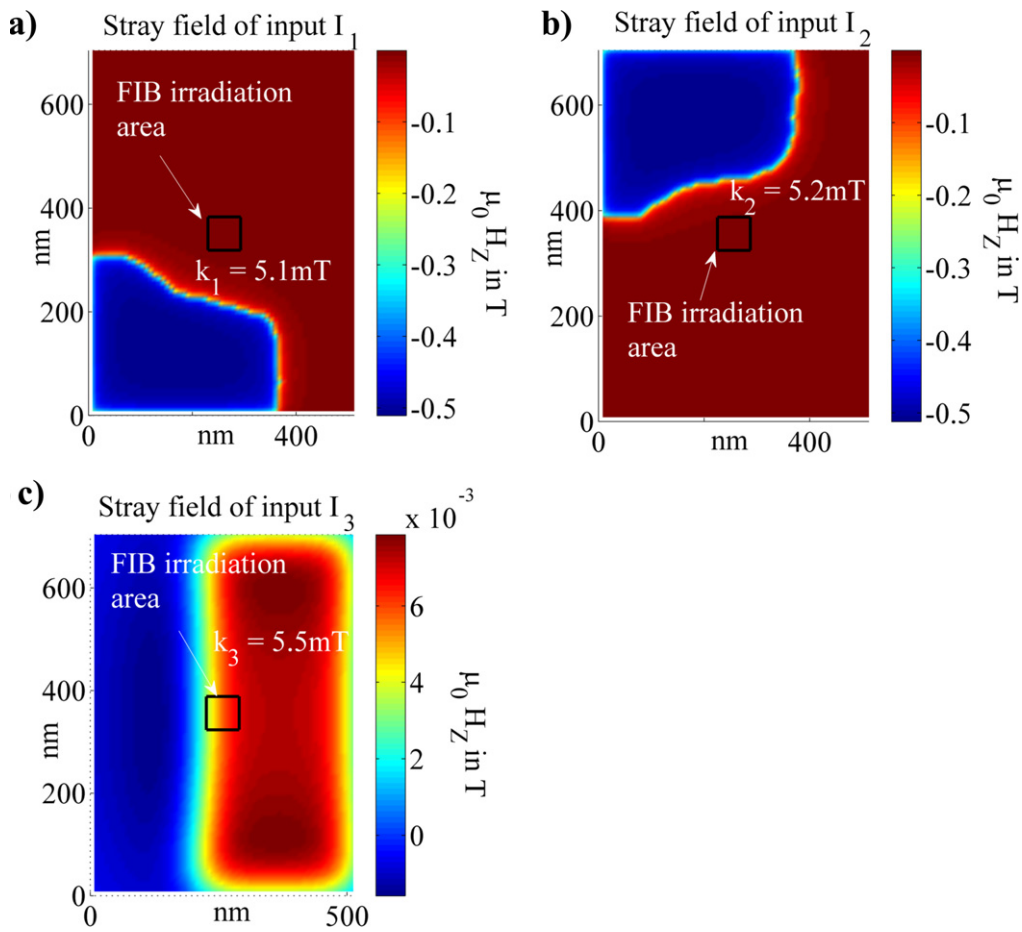


Figure 5. Simulation results for the stray fields of each gate input (reduced size, computing area). (a) Stray field of input I_1 . In the area where the irradiated spot of the output magnet is located, a stray field of $k_1 = 5.1$ mT is acting. (b) Stray field of input I_2 . In the area where the irradiated spot of the output magnet is located, a stray field of $k_2 = 5.2$ mT is acting. (c) Stray field of input I_3 in the height of 60 nm (output magnet is located 60 nm above I_3). In the irradiated area of the output magnet, the stray field amounts to 5.5 mT. The simulated stray field values are in very good agreement with the measured ones.

NAND/NOR gates, whereas the third input I_3 is located in an extra layer. I_3 programs the gate to a NOR or NAND. Its location in an extra layer provides the possibility to decouple programmable and computing operations of the circuit. Information between functional layers can be led up and

down by a magnetic via [27]. The magnetic via exploits magnetic field interaction of overlying magnets for signal transmission between functional layers. The magnetic via is also used for magnetic signal crossing [28]. To cross the signal of C_1 and C_3 , the magnetization state of C_1 is detoured

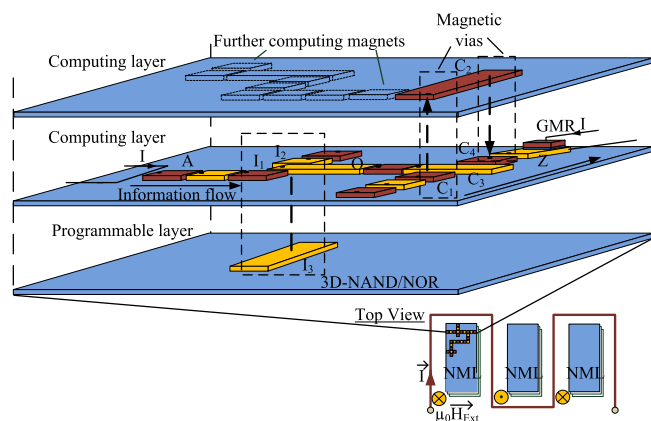


Figure 6. Schematic of a 3D NML system. Logic computing is performed by 3D NAND/NOR gates. Information between functional layers is transmitted by magnetic vias, enabling magnetic signal crossing and computing on a multi-level regime. Electrical in- and output sensors enable us to transform magnetic information into the electrical domain and vice versa.

through a further functional layer. Therefore, the magnetization state of C_1 is first transferred to magnet C_2 and then led back to its original layer to C_4 . For the electrical read out of magnetic signals (see magnet Z), e.g., Giant-Magneto-Resistance (GMR) [29], Magneto-Tunnel-Junction (MTJ) [29], or extraordinary Hall-Effect [30] sensors can be used. To clock the system, a magnetic field perpendicular to the film-plane is required. This clocking field can be generated by an on-chip inductor in the form of a meander [31] (see figure 6 (right bottom)). Several NML systems can be located in parallel, surrounded by the inductor. The whole system is then clocked by alternating field pulses with the same magnitude, on the condition that the switching field variations of the magnets can be reduced to a minimum to achieve an infallible clocking window [7]. Irradiation with He-ions promises improved control of domain wall injection [22] and may therefore offer a pathway for a better controllability of the switching field variations. Looking toward mass production, an ion projection direct structuring technique described in [32] can be used to perform FIB irradiation simultaneously at full disk surfaces. The irradiation spot itself can be reduced to $10\text{ nm} \cdot 10\text{ nm}$.

Of course, high integration densities lead to the problem that the stray fields of far-away magnets will add up to the stray fields of nearest neighbour magnets and cause errors in the field-interaction of neighbouring magnets and therefore signal processing. The reader is referred to the paper of Liu et al [33], where these problems are envisioned, discussed, and solutions provided.

5. Conclusion

We presented a programmable, non-volatile majority gate with a 3D architecture for magnetic logic computing. To prove the correct operation of the gate, we analyzed the switching behaviour of the output magnet for each of the

possible eight input magnetization configurations. MOKE measurements reveal that the net stray field emanating from the input magnets always force the output magnet in the correct alignment, while misalignment is always prohibited by the net stray field. Even in the presence of thermal noise and for a high number of switching cycles, the gate operated correctly. MFM images manifested the correctly computed magnetization state of the output magnet for each input configuration. Numerical simulations confirm that the computing area of the gate amounts to only $\approx 700\text{ nm} \cdot 550\text{ nm}$. In comparison to the 2D gate, the 3D arrangement of the magnets enables us to increase the influence of the input magnets on the output magnet, leading to a higher robustness of the gate. Furthermore, we proposed a whole 3D architecture for NML circuitry to enable magnetic logic computing on a multi-level regime. Magnetic computing takes place simultaneously in several functional layers, enabling the highest integration densities. The feasibility of 3D magnetic logic computing is demonstrated on the basis of the proposed 3D NAND/NOR gate.

Acknowledgments

The authors would like to thank the DFG (Grant SCHM 1478/9-2 and SCHM 1478/11-1) for financial support.

References

- [1] Cowburn R P and Welland M E 2000 *Science* **287** 1466–68
- [2] Allwood D A, Xiong G, Cooke M D, Faulkner C C, Atkinson D, Vernier N and Cowburn R P 2002 *Science* **296** 2003–6
- [3] Allwood D A, Xiong G, Faulkner C C, Atkinson D, Petit D and Cowburn R P 2005 *Science* **309** 1688–92
- [4] See www.itrs.net for ITRS: Emerging Research Devices (2011)
- [5] Cowburn R P 2006 *Science* **311** 183–4
- [6] Breitkreutz S, Kiermaier J, Ju X, Csaba G, Schmitt-Landsiedel D and Becherer M 2011 *Proc. European Solid-State Device Research Conf. (ESSDERC, 2011)* pp 323–26
- [7] Eichwald I, Bartel A, Kiermaier J, Breitkreutz S, Csaba G, Schmitt-Landsiedel D and Becherer M 2012 *IEEE Trans. Magn.* **48** 4332–35
- [8] Kiermaier J, Breitkreutz S, Eichwald I, Engelstädter M, Ju X, Csaba G, Schmitt-Landsiedel D and Becherer M 2013 *J. Appl. Phys.* **113** 17B902
- [9] Imre A, Csaba G, Ji L, Orlov A, Bernstein G H and Porod W 2006 *Science* **311** 205–8
- [10] Breitkreutz S, Kiermaier J, Eichwald I, Ju X, Csaba G, Schmitt-Landsiedel D and Becherer M 2012 *IEEE Trans. Magn.* **48** 4336–39
- [11] Varga E, Csaba G, Bernstein G H and Porod W 2011 *11th IEEE Int. Conf. on Nanotechnology (Portland)* pp 1244–47
- [12] Breitkreutz S, Kiermaier J, Eichwald I, Hildbrand C, Csaba G, Schmitt-Landsiedel D and Becherer M 2013 *IEEE Trans. Magn.* **49** 4464–67
- [13] Bhowmik D, You L and Salahuddin S 2013 *Nat. Nanotechnol.* **9** 59–63
- [14] Franken J H, Swagten H J M and Koopmans B 2012 *Nat. Nanotechnol.* **7** 499–503

- [15] Csaba G, Imre A, Bernstein G H, Porod W and Metlushko V 2002 *IEEE Trans. Nanotechnol.* **1** 209–13
- [16] Vieu C *et al* 2002 *J. Appl. Phys.* **91** 3103–10
- [17] Breitzkreutz S, Kiermaier J, Karthik S V, Csaba G, Schmitt-Landsiedel D and Becherer M 2012 *J. Appl. Phys.* **111** 07A715
- [18] DOW CORNING, XR-1541-004, E-Beam Resist in MIBK
- [19] Chen C-T and Chiou B-S 2004 *J. Mater. Sci.-Mater. Electron.* **15** 139–43
- [20] Chappert C *et al* 1998 *Science* **280** 1919–22
- [21] Aign T *et al* 1998 *Phys. Rev. Lett.* **81** 5656–59
- [22] Franken J H, Hoeijmakers M, Lavrijsen R, Kohlhepp J T, Swagten H J M, Koopmans B, van Veldhoven E and Maas D J 2011 *J. Appl. Phys.* **109** 07D504
- [23] Thomson T, Hu G and Terris B D 2006 *Phys. Rev. Lett.* **96** 257204
- [24] Engelen J B C, Delalande M, le Fèvre A J, Bolhuis T, Shimatsu T, Kikuchi N, Abelman L and Lodder J C 2010 *Nanotechnology* **21** 035703
- [25] Donahue M and Porter D 1999 OOMMF User's guide, version 1.0. *National Institute of Standards and Technology, Interagency Report NISTIR 6376*
- [26] Kiermaier J, Breitzkreutz S, Csaba G, Schmitt-Landsiedel D and Becherer M 2012 *J. Appl. Phys.* **111** 07E341
- [27] Eichwald I, Kiermaier J, Breitzkreutz S, Wu J, Csaba G, Schmitt-Landsiedel D and Becherer M 2013 *IEEE Trans. Magn.* **49** 4468–71
- [28] Eichwald I, Breitzkreutz S, Kiermaier J, Csaba G, Schmitt-Landsiedel D and Becherer M 2014 *J. Appl. Phys.* **115** 17E510
- [29] Mangin S, Ravelosona D, Katine J A, Carey M J, Terris B D and Fullerton E E 2006 *Nat. Mater.* **5** 210–15
- [30] Kiermaier J, Breitzkreutz S, Ju X, Csaba G, Schmitt-Landsiedel D and Becherer M 2011 *Solid-State Electron.* **65-66** 240–45
- [31] Becherer M, Kiermaier J, Breitzkreutz S, Eichwald I, Csaba G and Schmitt-Landsiedel D 2013 *IEEE Proc. 43rd European Solid-State Device Research Conf. (ESSDERC)* pp 276–79
- [32] Dietzel A *et al* 2002 *IEEE Trans. Magn.* **38** 1952–54
- [33] Liu S, Csaba G, Hu X S, Varga E, Niemier M T, Bernstein G H and Porod W 2013 *Proc. 50th Ann. Design Automation Conf.* vol 106 pp 1–7